JACS
JOURNAL OF THE AMERICAN CHEMICAL SOCIETY
pubs.acs.org/JACS
Article

# How Cell-Penetrating Peptides Behave Differently from Pore-Forming Peptides: Structure and Stability of Induced Transmembrane Pores

Haleh Alimohamadi, Jaime de Anda, Michelle W. Lee, Nathan W. Schmidt, Taraknath Mandal, and Gerard C. L. Wong*

Cite This: J. Am. Chem. Soc. 2023, 145, 26095−26105
Read Online
ACCESS | Metrics & More | Article Recommendations | Supporting Information

**ABSTRACT:** Peptide-induced transmembrane pore formation is commonplace in biology. Examples of transmembrane pores include pores formed by antimicrobial peptides (AMPs) and cell-penetrating peptides (CPPs) in bacterial membranes and eukaryotic membranes, respectively. In general, however, transmembrane pore formation depends on peptide sequences, lipid compositions, and intensive thermodynamic variables and is difficult to observe directly under realistic solution conditions, with structures that are challenging to measure directly. In contrast, the structure and phase behavior of peptide−lipid systems are relatively straightforward to map out experimentally for a broad range of conditions. Cubic phases are often observed in systems involving pore-forming peptides; however, it is not clear how the structural tendency to induce negative Gaussian curvature (NGC) in such phases is quantitatively related to the geometry of biological pores. Here, we leverage the theory of anisotropic inclusions and devise a facile method to estimate transmembrane pore sizes from geometric parameters of cubic phases measured from small-angle X-ray scattering (SAXS) and show that such estimates compare well with known pore sizes. Moreover, our model suggests that although AMPs can induce stable transmembrane pores for membranes with a broad range of conditions, pores formed by CPPs are highly labile, consistent with atomistic simulations.

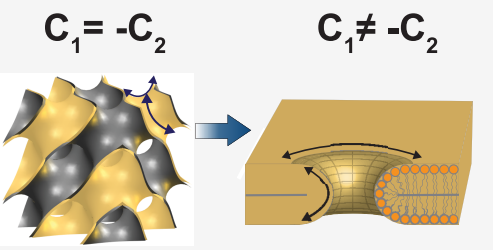


## INTRODUCTION

Transmembrane pore formation is central to biological processes critical to the maintenance of complex organisms, and the dysregulation of such processes results in a broad range of disease states. For example, peptides such as antimicrobial peptides (AMPs) can bind to bacterial membranes and disrupt the membranes through transmembrane pore formation, blebs, and vesiculation, which can lead to membrane depolarization, leakage, and cell lysis.[1−4] Bcl-2 family proteins integrate multiple surface stresses, such as hydrophobic insertion and oligomerization into putative supramolecular pores, to govern the intrinsic apoptotic pathway.[5] What's more, recent work has shown that histones and fragments thereof can lead to poration processes that precipitate smooth muscle cell death and inflammatory responses in atherosclerosis.[6] The membrane remodeling necessary for such pore formation is often accomplished via proteins or peptides, which adsorb or insert onto a cell membrane and thereby influence its geometry.

Direct experimental measurements of the pore geometry have been a challenge for decades. Several methods have been proposed to measure the radii of transmembrane pores in situ or in reconstituted systems, each with its own compromises. These include variations of dye leakage, atomic force microscopy (AFM), electron microscopy (EM), and small-angle X-ray scattering (SAXS).[2,7,8] Even with the availability of a structural model, the general expectation is that it is not one single static structure because the formation of transmembrane pores in realistic biological contexts depends on a protein or peptide sequence, lipid composition, and a broad range of intensive thermodynamic variables. Additionally, the size of pores in the membrane typically varies within the order of nanometers and changes with time and thermal fluctuations, which can render them challenging to measure experimentally. In electron-based structural probes, this difficulty is exacerbated by the potential for radiation damage, which can influence the equilibration of the system, and the intrinsic low signal-to-noise ratio, which can limit contrast in biological samples.[9]

SAXS is, in principle, a nondestructive technique that has been used extensively to study membrane remodeling at the nanoscale. Using SAXS experiments, it has been previously shown that various AMPs and cell-penetrating peptides (CPPs) can restructure small unilamellar vesicles (SUVs)

Received: July 26, 2023
Revised: November 2, 2023
Accepted: November 3, 2023
Published: November 21, 2023







https://doi.org/10.1021/jacs.3c08014
J. Am. Chem. Soc. 2023, 145, 26095−26105

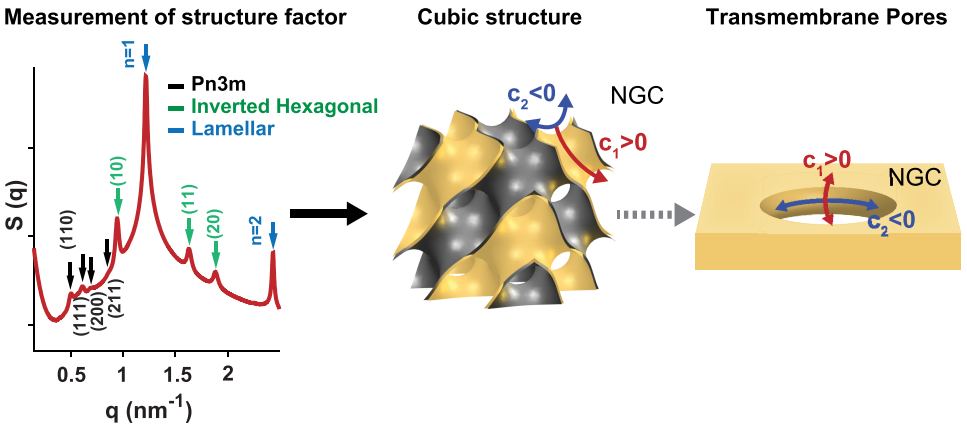


**Figure 1.** Using induced membrane curvature deformations by NGC-generating inclusions in SAXS spectra to estimate the radius of transmembrane pores generated by pore-forming peptides. Cubic structure and transmembrane pores are both characterized by a saddle shape (NGC) with positive and negative principal curvatures ($c_1 > 0$ and $c_2 < 0$).

into bicontinuous cubic phases, which are rich in negative Gaussian curvature (NGC).[10−18] In a more general compass, NGC is required to allow communication through a membrane: it has been shown that cubic lipid matrices can be used to promote efficient siRNA delivery.[19,20] This observed behavior is, in principle, consistent with their biological membrane remodeling activity since NGC or saddle splay curvature is topologically required for the formation of transmembrane pores. However, it is not clear how to correlate the measured induced curvatures in the cubic phases (such as the NGC density per volume) to the actual size of transmembrane pores in the membrane (Figure 1). Indeed, cubic phases are idealized as minimal surfaces with zero mean curvature so that the principal curvatures $c_1$ and $c_2$ are equal in magnitude but opposite in sign at every point (Figure 1), a condition that is not met (a least in general) for typical transmembrane pores, which have extremely high positive curvature $c_1$ ($\sim$1/2 nm$^{-1}$).

In recent years, discrete and continuum theoretical approaches combined with information from experiments have emerged as a powerful method to study the induced membrane curvatures by proteins and peptides.[21−30] Discrete models are powerful for exploring the molecular mechanisms underlying lipid−peptide interactions. In contrast, continuum models work best when engaging membrane phenomena on large scales, such as processes that require membrane deformations over hundreds of nanometers. For example, Akimov et al. applied continuum elasticity theory to analyze the energy landscape of pore formation and closure.[31,32] They proposed that the magnitude of line tension at the edge of a transmembrane pore depends on the radius of the pore and external surface stresses.[31,32] Betterton et al. studied the competition between electrostatics effects and line tension in opening a transmembrane pore, and later Fošnarič et al. showed the ability of anisotropic inclusions to stabilize transmembrane pores in the membrane.[33,34] However, it is not clear how to generalize these methods to estimate pore sizes from SAXS experiments for different protein-peptide sequences, pH conditions, or temperatures.

In this work, we present a minimal mechanical model at the continuum length scale to estimate the radius of peptide-induced transmembrane pores based on peptide-induced membrane deformations measured in SAXS experiments conducted specifically for different peptide sequences, temperature, or other intensive thermodynamic variables. Specifically, we estimate the magnitude of induced curvatures by peptides from measured lattice constants of cubic phases and minimize the excess free energy of transmembrane pore formation by leveraging a model based on anisotropic membrane inclusions. We systematically explore the influence of the cubic lattice constant, peptide surface area, electrostatic repulsion, and interfacial tension at the pore's edge on the opening and closure of transmembrane pores. The model indicates that the pore radius is a nonmonotonic function of the cubic lattice constant; the pore radius initially increases with the cubic phase lattice constant but eventually saturates and then decreases. We show that the pore radii calculated with our model are in agreement with the experimental measurements. Furthermore, this mechanical framework is used to estimate the sizes of pores generated by AMPs and CPPs and analyze the stability of these induced pores to variations in the membrane properties. Interestingly, we find that transmembrane pores induced by CPPs are intrinsically much more labile than those induced by AMPs when membrane perturbations are considered. These results are consistent with those from atomistic simulations and independent of effects from peptide residence time in the membrane. We believe our proposed framework can be generalized to other pore-forming systems and can potentially provide insight into the development of new antimicrobials and drug-delivery systems.

## MODEL DEVELOPMENT

**Membrane Mechanics.** Our system consists of a lipid membrane and NGC-generating inclusions (proteins or peptides) confined in the saddle-shaped domain at the rim of transmembrane pores. Previous studies have shown that AMPs have a stronger binding affinity for the pore domain in order to stabilize pore formation.[35] In this study, we model the lipid bilayer as a continuous elastic shell with negligible thickness and assume that the membrane is areally incompressible.[36−38] This allows us to simplify the total free energy of the system ($E_{total}$) as[33,34,39−41]

$$E_{total} = E_{interaction} + E_{line\ tension} + E_{electrostatic} \quad (1)$$

where $E_{interaction}$ is the elastic energy due to the mismatch between the local shape of the lipid membrane and the intrinsic shape of the inclusion, $E_{line\ tension}$ is the energy cost due to the exposure of the hydrophobic tails of lipid molecules



https://doi.org/10.1021/jacs.3c08014
J. Am. Chem. Soc. 2023, 145, 26095−26105

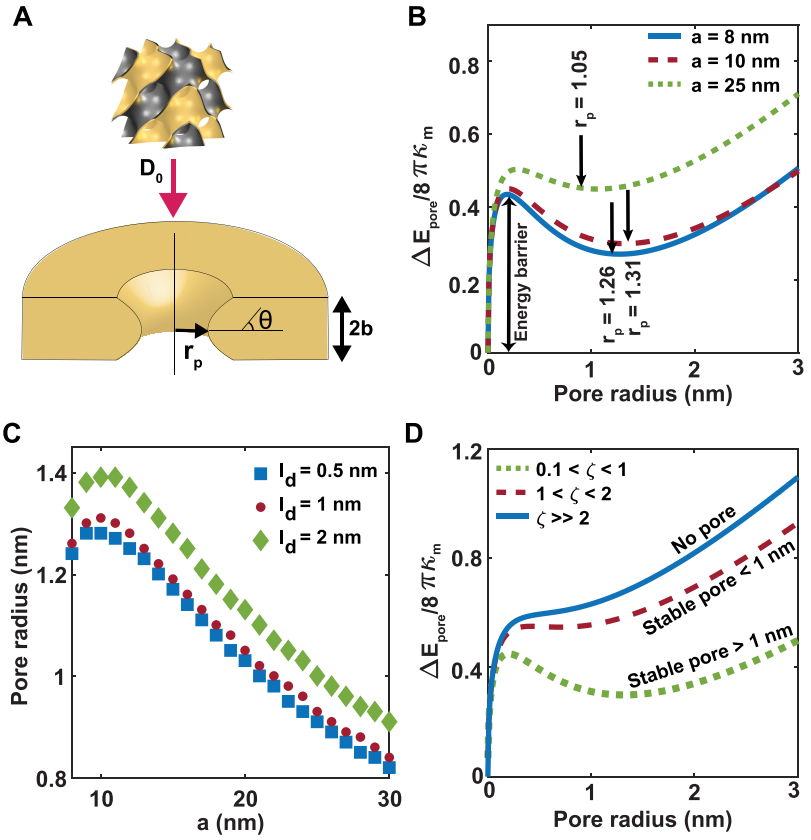


**Figure 2.** Estimating the radius of transmembrane pores induced by pore former peptides based on the generated cubic structures in SAXS experiments. (A) Induced deviatoric curvature ($D_0$) in a cubic structure by a pore former peptide is used to estimate the radius of a circular pore in a planar membrane. The transmembrane pore is modeled as a semitoroidal cap with a radius of $r_p$ and a height equal to the bilayer thickness $2b$ ($\pi/2 < \theta < 3\pi/2$). (B) Change in the energy of the system from a planar membrane with no pore to a planar membrane with a single circular pore (eq 5) as the function of the pore radius for three different lattice constants ($a_p/2$ = 6 nm$^2$, $\sigma$ = −0.05 As/m$^2$, and $l_d$ = 1 nm, $\gamma$ = 10 pN, and using $Pn3m$). Arrows show the location of minimum energy that corresponds to the radius of a stable transmembrane pore formed in the membrane. (C) Nonmonotonic function of pore radius with increasing the cubic lattice constant ($a_p/2$ = 6 nm$^2$, $\sigma$ = −0.05 As/m$^2$, and $\gamma$ = 10 pN). (D) Change in the energy of the system as a function of pore radius for different ratios of Debye length to the peptide surface area and induced deviatoric curvature, $\zeta = l_d/(a_p \times D_0)$ ($\sigma$ = −0.05 As/m$^2$ and $\gamma$ = 10 pN).

at the edge of the transmembrane pore, and $E_{electrostatic}$ is the electrostatic repulsion energy between the charged lipids around the pore. Assuming that the membrane inclusions are more rigid than the lipid bilayer and impose their intrinsic curvatures on the underlying membrane,[42,43] the membrane-inclusion interaction energy is given as[39−41]

$$E_{interaction} = \int (2K_{1,p} + K_{2,p})(H - H_0)^2 n a_p - K_{2,p}(D - D_0)^2 n a_p dA \quad (2)$$

where $K_{1,p}$ and $K_{2,p}$ are constants ($K_{1,p} > 0$ and $K_{2,p} < 0$) representing the strength of interaction between the inclusions and the surrounding membrane.[39,40] $H$ is the mean curvature of the membrane, and $D$ denotes the curvature deviator of the lipid membrane ($H^2 - D^2 = K$ is the Gaussian curvature).[44] $H_0$ and $D_0$ are the intrinsic mean and deviatoric curvatures of the inclusion, respectively. $a_p$ is the area of the inclusion in contact with the surrounding membrane, and $n$ is the density of the inclusions on the membrane surface. In eq 2, we assume that attached inclusions have a homogeneous lateral distribution on the surface and impose their intrinsic curvatures on the underlying membrane[39,45] and the integral is taken over the area of the membrane that is covered by NGC-generating inclusions.

The interfacial energy at the edge of the transmembrane pore in eq 1 is given as

$$E_{line\ tension} = \gamma \oint dl \quad (3)$$

where $\gamma$ is a constant representing the magnitude of the interfacial force and the integral is taken over the interfacial line $\partial l$. The line tension energy favors closing the transmembrane pores in the lipid bilayers. The magnitude of line tension ($\gamma$) depends on various factors, such as the lipid composition,[46−49] the radius of the pore,[31] the interaction between the membrane and inclusions such as AMPs,[50] and external stresses applied to the membrane.[32] Here, for simplicity, we assume that the line tension is constant and independent of the lipid composition or membrane morphology.

We model the electrostatic repulsion energy in eq 1 using the linearized Poisson−Boltzmann formalism for thin membranes, which is given by[33,34,51,52]

$$E_{electrostatic} = \frac{-\pi\sigma^2 r_p^2}{\varepsilon_w \varepsilon_0 k_d} + \frac{2\pi\sigma^2 r_p^3}{\varepsilon_w \varepsilon_0} \int_0^\infty \frac{J_1(x)^2}{x\sqrt{x^2 + k_d^2 r_p^2}} dx \quad (4)$$



https://doi.org/10.1021/jacs.3c08014
J. Am. Chem. Soc. 2023, 145, 26095−26105

where $\sigma$ is the surface charge density, $r_p$ is the radius of a pore, $\varepsilon_0$ is the permittivity of free space, $\varepsilon_w \approx 80$ is the dielectric constant of the aqueous solution, $k_d$ is the inverse of Debye length ($k_d^{-1} = l_d$), and $J_1$ is the Bessel function. Electrostatic energy favors the opening and enlargement of the transmembrane pores. It should be mentioned that the LPB approximation is valid for sufficiently small surface charge density in physiological salt concentrations while it greatly overestimates the electrostatic free energies.[34]

To establish the relationship between the induced curvatures by pore former peptides observed in SAXS experiments and the radius of the stable transmembrane pores, we assume that pore former peptides generate a single circular pore with a radius of $r_p$ on a planar membrane. We model the transmembrane pore as a semitoroidal cap with a height equal to the bilayer thickness (2b, Figure 2A) and write the excess free energy with respect to a flat membrane with no pore as

$$\Delta E_{pore}(r_p) = \frac{-2\pi\sigma^2 r_p^2}{\varepsilon_w\varepsilon_0 k_d} + \frac{4\pi^2\sigma^2 r_p^3}{\varepsilon_w\varepsilon_0}\int_0^\infty \frac{J_1(x)^2}{x\sqrt{x^2 + k_d^2 r_p^2}}dx + 2\pi\gamma r_p + \frac{(2K_{1,p} + K_{2,p})r_p\sqrt{a_p}}{4\left(\pi r_p + \pi b - 2b\right)} \int_{\frac{\pi}{2}}^{\frac{3\pi}{2}} \left(\frac{1}{b} + \frac{\cos(\theta)}{r_p + b(1+\cos(\theta))}\right)^2 (r_p + b(1+\cos(\theta)))d\theta - \frac{K_{2,p} r_p\sqrt{a_p}}{4\left(\pi r_p + \pi b - 2b\right)} \int_{\frac{\pi}{2}}^{\frac{3\pi}{2}} \left(\frac{1}{b} - \frac{\cos(\theta)}{r_p + b(1+\cos(\theta))} - D_0\right)^2 (r_p + b(1+\cos(\theta)))d\theta \quad (5)$$

where $\theta$ is the angle between the vertical axis and the boundary of the semitoroidal cap. It should be mentioned in eq 5, we assume that the induced mean curvature by NGC-generating inclusions is negligible compared to the induced deviatoric curvature ($H_0 \ll D_0$) and also restrict the number of inclusions in the rim region based on the steric repulsions between inclusions ($N_{max} = \pi r_p/\sqrt{a_p}$)[33]

We estimate the magnitude of the induced deviatoric curvature ($D_0$ in eq 5) by NGC-generating inclusions based on the identified cubic structures in SAXS measurements given as[53,54]

$$D_0|_{\text{energy min ization}} = \langle D\rangle = \sqrt{\frac{2\pi\chi}{A^* a^2}} \quad (6)$$

where $a$ is the lattice parameter, $\chi$ is the Euler characteristic, and $A^*$ is the surface area per unit cell specific to each cubic phase.[53,54] Using SAXS data, we can determine the type of cubic phases and their corresponding lattice constants, which allows us to calculate the magnitude of the induced curvatures (Figure 2A). Assuming that the magnitude of the induced deviatoric curvature by pore former peptides is independent of the peptide−lipid system, we apply derived $D_0$ from SAXS data to a planar membrane with a toroidal pore with a radius of $r_p$. Assuming that the total area of the membrane remains constant, we numerically calculate the excess energy of the planar membrane system (eq 5) and find the pore radius that minimizes this energy. Biologically relevant values for the parameters that have been used in the mathematical model are given in Table S1. Particularly, the surface charge density and Debye length are set for a range of valid LPB approximation using physiological monovalent salt concentration of 25−100 mM.[34] We also estimate the strength of interaction between the membrane and inclusions using the elastic properties of the membrane and the characteristic length of the inclusions (eqs S13−S15).

## RESULTS AND DISCUSSION

**Estimation of the Radius of Transmembrane Pores Generated by Pore-Forming Peptides.** A range of peptides can remodel lipid membranes and open transmembrane pores. The size of transmembrane pores induced by peptides is a key geometric parameter in mediating different processes such as apoptosis, cell death, and pathogen internalization.[16,55] Here, we use our mechanical framework to estimate the radius of transmembrane pores induced by pore former peptides from SAXS measurements and systematically explore the influence of cubic lattice constant, projected peptide surface area on the membrane, interfacial tension, and charge density on the size of the generated pores.

We used the deviatoric curvature ($D_0$) directly extracted from lattice constants of *Pn*3*m* cubic structures measured in SAXS as input to a planar membrane with a semitoroidal pore (Figure 2A). We minimized the energy of the system, as described in eq 5. The change in the energy has a local minimum, which represents the formation of a stable semitoroidal pore in the membrane with the presence of NGC-generating inclusions (Figure 2B, $a_p/2 = 6$ nm$^2$, $\sigma = -0.05$ As/m$^2$, $l_d = 1$ nm, and $\gamma = 10$ pN). We observed that pore formation in the membrane is associated with an energy barrier, and the height of the energy barrier increases as the lattice constant of the cubic phase decreases, or, in other words, the induced deviatoric curvature increases (Figure 2B). This energy barrier characterizes the transition from a hydrophobic defect into a hydrophilic pore.[31,56]

Using the Gauss−Bonnet theorem, the energy barrier associated with the pore formation is estimated as $\Delta E_{barrier} = -4\pi\kappa_G$, where $\kappa_G$ is the Gaussian modulus of the membrane. Simplifying the elastic membrane−peptide interactions energy for a toroidal-shaped pore, we showed that the induced deviatoric curvature by NGC-generating peptides can lower the energy barrier required for pore formation as $\Delta E_{barrier} = -4\pi\kappa_G[1 - D_0\sqrt{br_p}(2 - D_0\sqrt{br_p})]$ (eq S8). Additionally, for membranes with no inclusions, previous studies have shown that the local minimum of the energy for transmembrane pore formation is shallow (below $kT$) and the pore likely closes from thermal fluctuations.[33,34] However, partitioning of anisotropic inclusions such as pore-forming peptides (e.g., AMPs) in the membrane rim can significantly lower and deepen the local minimum of the energy, which leads to the formation of stable and long-lasting transmembrane pores.[16] Thus, anisotropic pore former peptides not only reduce the energy barrier of the pore formation but also stabilize the induced pores on the membrane.

It is interesting to note that the radius of the pore is a nonmonotonic function of the cubic lattice constant. As the


https://doi.org/10.1021/jacs.3c08014
J. Am. Chem. Soc. 2023, 145, 26095−26105

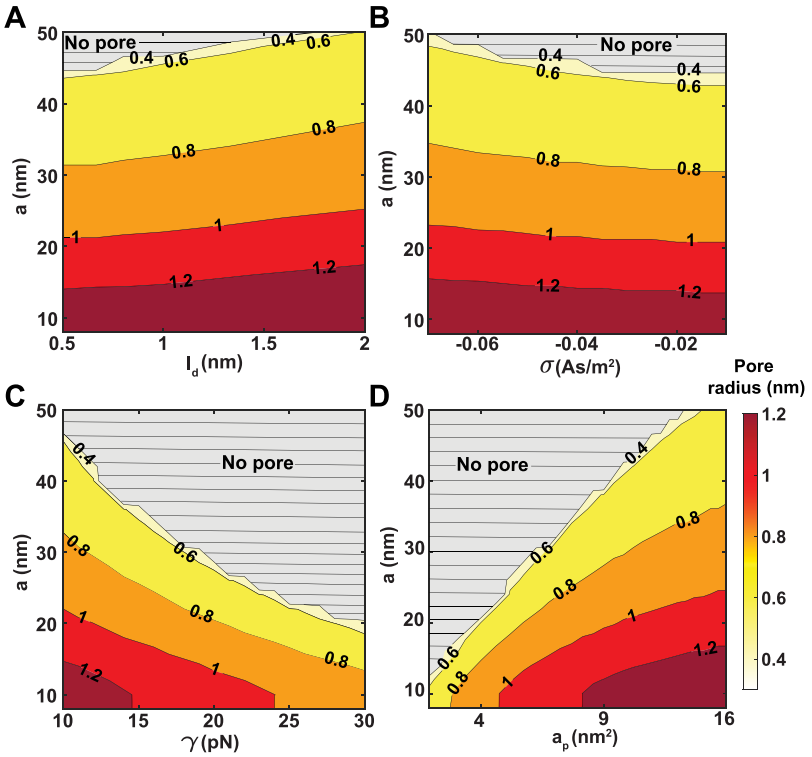


**Figure 3.** Size of transmembrane pores depends on the cubic lattice constant ($a$), charge density ($\sigma$), line tension ($\gamma$), and the surface area of the peptide ($a_p$). Contour plot of the transmembrane pore radius for a range of (A) cubic lattice constants and Debye length ($\sigma = -0.05$ As/m$^2$, $a_p/2 = 6$ nm$^2$, and $\gamma = 10$ pN), (B) cubic lattice constants and charge density ($l_d = 1$ nm, $a_p/2 = 6$ nm$^2$ and $\gamma = 10$ pN), (C) cubic lattice constants and line tension ($\sigma = -0.05$ As/m$^2$, $a_p/2 = 6$ nm$^2$, and $l_d = 1$ nm), (D) cubic lattice constants and peptide surface area ($\sigma = -0.05$ As/m$^2$, and $l_d = 1$ nm, and $\gamma = 10$ pN). The gray domains in panels (A−D) mark the regions with no pores.

cubic lattice constant increases, the radius of the pore increases, saturates, and then decreases (Figure 2C, $a_p/2 = 6$ nm$^2$, $\sigma = -0.05$ As/m$^2$, and $\gamma = 10$ pN). This can be due to the different distribution of anisotropic curvature in a semitoroidal pore versus a cubic phase: The principal curvatures within a transmembrane pore are strong anisotropic: A large positive curvature is necessary for the lip that connects the outer leaflet with the inner leaflet, whereas a range of negative curvatures can be accommodated in the circumference of the pore. This contrasts with curvatures in a cubic phase, where the positive and negative curvatures are constrained to be equal in magnitude. Moreover, our results showed that the non-monotonic relationship between the pore radius and the cubic lattice constant becomes even more prominent with an increase in Debye length (Figure 2C), surface charge density (Figure S1A), and the surface area of the peptide in contact with membrane (Figure S1B), and a decrease in the interfacial line tension (Figure S1C).

We identified three different regimes of pore-forming behavior, depending on the ratio of the Debye length to the surface area of the pore former peptide and induced deviatoric curvature, $\zeta = l_d/(a_p \times D_0)$. In Figure 2D, we plotted the change in the energy of the membrane as a function of the pore radius for a fixed surface charge density and line tension ($\sigma = -0.05$ As/m$^2$ and $\gamma = 10$ pN). (I) At small $\zeta$ ($0.1 < \zeta < 1$), the change in energy is minimized for a large pore radius, $r_p > 2$ nm (dotted green line in Figure 2D). (II) At intermediate $\zeta$ ($1 < \zeta < 2$), the energy is minimized at a small pore radius, $r_p \sim 1$ nm (dashed red line in Figure 2D). (III) At large $\zeta$ ($\zeta \gg 2$), the change in energy increases with increasing radius of the pore, indicating that the holes always tend to close (solid blue line in Figure 2D). These results suggest that pore-forming peptides can generate large and stable holes in lipid membranes through conformational changes to alter the peptide−membrane contact surface area.

**Transmembrane Pore Formation Exists over a Range of Cubic Lattice Constants, Debye Length, Surface Charge Density, Line Tension, and Peptide Surface Area.** Over what ranges of cubic lattice constants, surface charge density, and line tension can peptides with different sizes open a stable transmembrane pore? To answer this question, we performed numerical calculations and calculated the radius of a stable transmembrane pore for a range of measured lattice constants in SAXS experiments, surface charge density, and Debye length for physiological monovalent salt concentration, as well as over a range of hydrophobic line tensions and surface area of peptides. The results are summarized in a series of "phase diagrams" (Figure 3A−D). The gray regions in Figure 3A−D represent the areas with no pore.

For physiological monovalent salt concentration, the Debye length and surface charge density vary in a wide range between $0.5 < l_d < 2$ nm[57,58] and $-0.01 < \sigma < -0.07$ As/m$^2$,[51] respectively. As expected from eq 4, with increasing the Debye length and the magnitude of surface charge density, the electrostatic repulsion becomes dominant, which results in the formation of larger pores in the membrane (Figure 3A,3B). Another factor that controls the size of the pore is induced line tension at the edge of the pore. The magnitude of line tension varies widely between $10 < \gamma < 200$ pN, depending on the lipid composition, particularly the molar fraction of cholesterol.[47,59,60] Our results show that line tension significantly


https://doi.org/10.1021/jacs.3c08014
J. Am. Chem. Soc. 2023, 145, 26095−26105

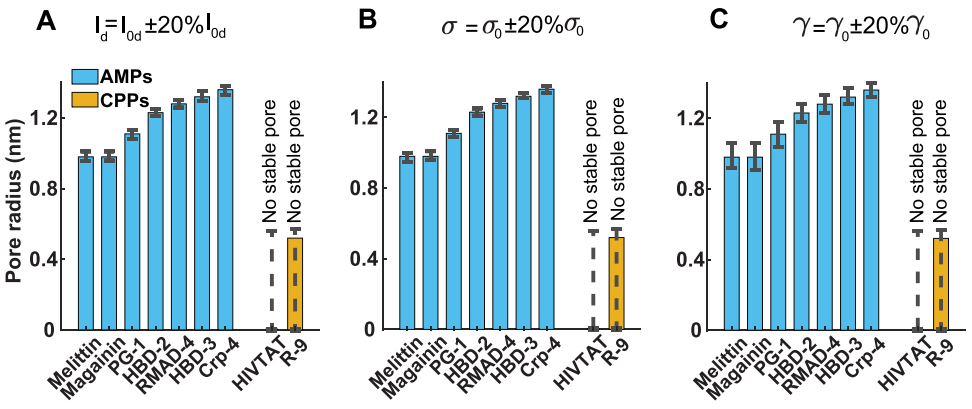


**Figure 4.** Sensitivity analysis of pore sizes induced by AMPs and CPPs to variation in the membrane properties. We used the measured cubic lattice constants of AMPs[13−16] and CPPs[10] in our previous studies and calculated the pore radius (eq 5) with 20% variation in (A) the Debye length ($l_d$), (B) the surface charge density ($\sigma$), and (C) the line tension ($\gamma$). $l_{0d}$ = 1 nm, $\sigma_0$ = −0.05 As/m$^2$, and $\gamma_0$ = 10 pN. AMPs are robust in generating stable pores with variations in membrane properties.

reduces the elongated length of the transmembrane pores. For example, for fixed $\sigma$ = −0.05 As/m$^2$, $a_p/2$ = 6 nm$^2$, and $l_d$ = 1 nm, almost no pore can be formed in the membrane when $\gamma$ > 25 pN for lattice constant >20 nm (Figure 3C).

Previous studies have shown that the structure and conformational stability of pore-forming peptides are key factors determining their antimicrobial activity.[61−63] To explore the relationship between the peptide structure and its antimicrobial activity, we estimated the induced pore sizes for a range of peptide contact surface areas with the membrane and cubic lattice constants (Figure 3D). The surface area of the peptides affects the strength of the membrane−peptide interactions (eq S13), and it also characterizes the number of peptides that can fit within the membrane rim due to steric repulsions.[16] We observed that the pore radius increases continuously with an increase in the surface area of the peptide (Figure 3D). Overall, our results provide important insights into the synergistic role of electrostatic repulsions, interfacial forces, and induced curvature by peptides in controlling the formation of stable pores in the membrane.

**Membrane Remodeling Behavior of AMPs and CPPs: Numerical Comparisons of Robustness of Induced Transmembrane Pores Using Continuum Framework.** Having established a mathematical model to estimate the size of membrane holes generated by pore-forming peptides from the induced cubic structures in SAXS experiments, we applied the framework to explore (I) the range of pore sizes induced by AMPs and CPPs and (II) the robustness of the formed pores against variations in the membrane properties. In our previous work, we utilized binary lipid mixtures (PS/PE 20/80 or PG/PE 20/80) and measured the lattice constant of cubic phases induced by AMPs including melittin, magainin (Figure S2), protegrin-1 (PG-1), human-$\beta$-defensin-2 (HBD-2), rhesus-myeloid-$\alpha$-defensin-4 (RMAD-4), HBD-2, mouse-$\alpha$-defensin-4 (CRP-4), and CPPs such as HIV TAT and R-9.[13,10,14−16] Using the reported cubic lattice constants and estimating the effective surface area of pore-forming peptides based on their amino acid sequence and structures, we calculated the radius of membrane pores generated by a variety of AMPs and CPPs for fixed $l_d$ = 1 nm, $\sigma$ = −0.05 As/m$^2$, and $\gamma$ = 10 pN (Table S2).

Based on our results, AMPs can induce stable transmembrane pores with a radius between 1 and 1.4 nm, which is in agreement with experimental measurements of pore sizes (Table S2).[22,28,64−68] However, our model predicts that CPPs, R-9, and HIV TAT, induce small pores that are not stable in the membrane (Table S2). Previous experimental studies have also suggested that CPPs such as R-9 can only generate transient pores, and HIV TAT peptides are only capable of inducing pores with high concentration and in model membranes that contain a significant proportion of anionic lipids or lipids that induce negative intrinsic curvatures.[64,68] Similarly, it has been suggested that cell-penetrating peptide pep-1 translocates across the cell membranes without forming a stable pore.[22,28,65,66] It is not clear, however, whether these labile pores are a consequence of expected shorter membrane residence times of cell-penetrating peptides, which typically have much less hydrophobicity than AMPs.

To investigate the intrinsic stability of the induced transmembrane pores of a specific pore size against variation in membrane properties, we introduced a 20% perturbation in the Debye length ($l_d$), the surface charge density ($\sigma$), and the line tension ($\gamma$) and then calculated the resulting pore radius (Figure 4). Interestingly, we found that AMPs display a high degree of stability in generating membrane pores across a range of membrane properties (Figure 4). With 20% variation in membrane properties, we observed that the radius of induced pores by AMPs slightly changes. However, our results indicate that formed "pores" by CPPs are highly unstable with respect to perturbations in environmental parameters (Figure 4). We hypothesize that such instability is intrinsic to small radii pores induced by CPPs, due to the strong elastic restoring forces from high local membrane curvature deformations. This instability makes measuring the accurate size of formed pores by CPPs challenging, considering that CPPs usually induce small transient pores in the membrane.[64,68] Thus, our framework predicts a transition in the character of the pores as the pore radius decreases from large stable pores from AMPs to labile pores from CPPs. More generally, from a methodological perspective, we have presented a minimal theoretical framework for (I) estimating pore size from the structure of induced cubic phases in SAXS, (II) analyzing the stability of pores against perturbations in the lipid bilayer properties, and (III) designing a reconstituted system in order to induce a desired pore size with a given pore-forming peptide or protein.

**Comparison of the Stability of Transmembrane Pores Induced by AMPs and by CPPs, Using Atomistic**


https://doi.org/10.1021/jacs.3c08014
J. Am. Chem. Soc. 2023, 145, 26095−26105

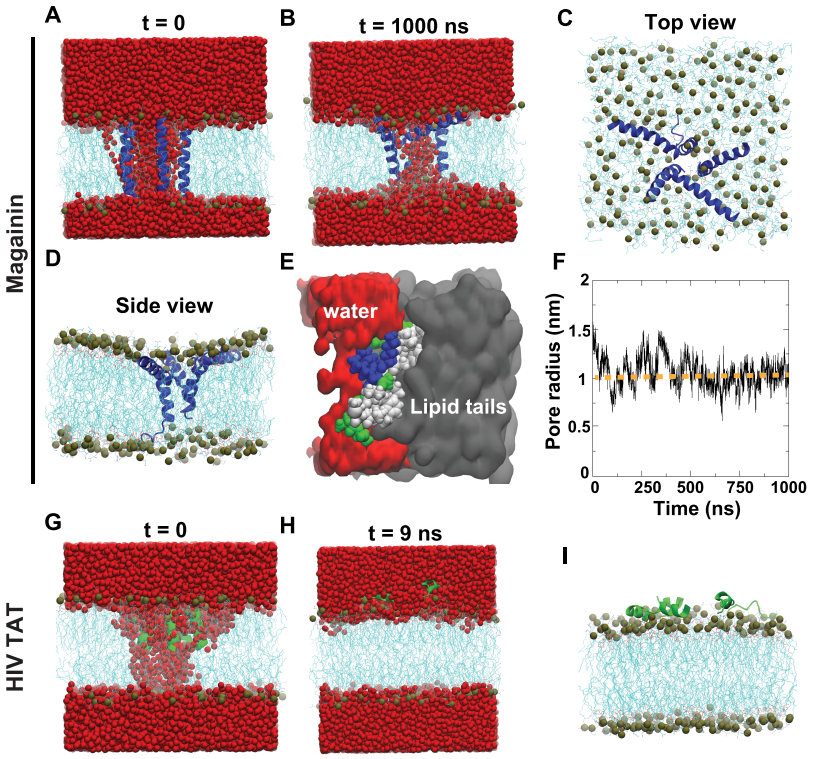


**Figure 5.** Molecular dynamic simulations to investigate the pore stabilization capability of magainin AMP versus HIV TAT CPP. (A) Structure of the preformed transmembrane pore with five magainin peptides at the beginning of the simulation. (B) Equilibrated structure of the transmembrane pore after 1000 ns long MD simulation. (C) Top and (D) side view of the equilibrated membrane pore without water molecules. Blue and cyan colors represent peptides and lipids, respectively. Oxygen atoms of the water molecules are shown by red spheres. Bile spheres represent the phosphorus atoms of the lipid heads. (E) Zoomed-in image of the pore structure shows that the hydrophobic residues (white) bind with the lipid tails (gray), and the hydrophilic residues (blue and green) are in contact with the water (red). Lipids and water are shown in the "surf" representation. (F) Radius of the pore as a function of simulation time. (G) Structure of the preformed transmembrane pore with five HIV TAT peptides at the beginning of the simulation. (H) Membrane pore closes within only 9 ns of equilibration. (I) Side view of the membrane after the closure of the pore,and the peptides move out from the membrane core. Green and cyan colors represent the HIV TAT peptide and the lipids, respectively.

**Molecular Dynamic Simulations.** Our results from the continuum framework suggest that AMPs but not CPPs have the ability to induce stable transmembrane pores. To test this hypothesis, we conducted fully atomistic Molecular Dynamic (MD) simulations using both AMPs and CPPs. Previous studies have revealed spontaneous pore formation in membranes by AMPs is challenging to achieve in fully atomistic simulations because, as we have shown in Figure 2, pore formation is associated with a high energy barrier.[27] Therefore, we investigate if AMPs and CPPs can stabilize a preformed membrane pore, which in the absence of any peptide undergoes spontaneous closure. We first constructed a transmembrane pore with five magainin AMPs in a DOPS/DOPE (20/80) bilayer (Figure 5A). Then, the bilayer was equilibrated through molecular dynamic (MD) simulations (see atomistic MD method in Supporting Information).

Our results show that embedded magainin peptides spontaneously readjusted their positions during equilibration to form a stable transmembrane pore (Figure 5B). Three out of the five peptides lined up along the water channel, and the remaining two adopted a tilted configuration near the pore edge, forming a semitoroidal-shaped transmembrane pore (Figure 5C,D). The amphipathic characteristics of the AMPs contribute to stabilizing the membrane pore, where the hydrophobic residues are in contact with the hydrophobic core of the membrane and the hydrophilic residues face the water channel (Figure 5E). We also calculated the radius of the pore as a function of simulation time to gain insights into the dynamics of the pore (Figure 5F). Based on our results, the water channel remained stable throughout the 1000 ns long MD simulation, and the radius of the pore was ∼1 nm, which is in good agreement with experimental data.[2,65,66] We also performed a control simulation by removing the magainin peptides from the preformed membrane pore and equilibrating the structure. We observed that the pore closed immediately within only 2 ns, confirming the role of magainin AMPs in stabilizing the transmembrane pore (Figure S3).

Next, we repeated the simulations with five HIV TAT CPP, following the same protocol described earlier (Figure 5G). In contrast to AMPs, we observed that the transmembrane pore was not stable (Figure 5H). The peptides moved out from the membrane core, resulting in the closure of the pore within a short time of 9 ns (Figure 5H,I). This finding suggests that HIV TAT peptides can generate transient pore morphologies probably due to their strong interactions with the anionic lipids.[68] However, they are unable to stabilize the induced pore due to the lack of hydrophobic residues that can bind with the lipid tails. Our MD simulation findings are in agreement with the experimental study by Kubitscheck et al. that reported the accumulation of HIV TAT peptides on an anionic GUV, leading to transient pore formation and rapid translocation of the peptides across the membrane. However, the lifetime of the


https://doi.org/10.1021/jacs.3c08014
J. Am. Chem. Soc. 2023, 145, 26095−26105

generated transmembrane pores was too short to be detected by single-molecule tracking.[68] Taken together, our molecular dynamic simulations and theoretical results suggest that AMPs are more robust than CPPs in generating and stabilizing the process of transmembrane pore formation.

In summary, by constructing a minimal mechanical model combined with information from SAXS measurements, we are able to estimate the radius of transmembrane pores. We systematically investigate the synergetic effects of the peptide surface area in contact with the membrane, the magnitude of curvatures induced by peptides, and the physical properties of the lipid membrane in governing the size of transmembrane pores (Figures 2 and 3). By leveraging SAXS measurements across different lipid compositions and pH, we are able to examine the fundamental determinants of pore formation from a new perspective. We find that the size of a transmembrane pore is a nonmonotonic function of the cubic lattice constant; as the lattice constant of the cubic phase increases, the pore radius increases, saturates, and then decreases (Figure 2). We also identify the range of lipid membrane physical properties combined with the surface area of peptides and induced curvatures to generate stable transmembrane pores (Figure 3). Additionally, we find that pores induced by AMPs are drastically more stable than those induced by CPPs, just from the standpoint of curvature elasticity, independent of the membrane residence times of peptides of different hydrophobicities (Figure 4). Atomic molecular dynamic simulations validated our predictions that AMPs but not CPPs can stabilize transmembrane pores for a long period of time (Figure 5).

It is interesting to note that CPPs are typically short with molecular lengths comparable to the elastic decay length of the membrane. Moreover, CPPs typically have fewer hydrophobic residues that insert into hydrophobic cores of membranes compared to AMPs. These observations imply that CPPs will tend to have weak interactions with the membrane (eq S15). We expect these effects to synergize with the results presented above on the size dependence of pore stability and thereby render high curvature pores even less stable, as indicated in atomistic simulations. Finally, we anticipate that results here are generalizable to pore-forming proteins such as viral fusion proteins[69,70] and a much broader repertoire of molecules, including synthetic molecules not based on amino acids.

**Limitations of the Model.** We acknowledge that despite the agreement with experimental data and our model predictions, there are some limitations and simplifying assumptions that will need to be revisited for future studies. First, we focused on the induced bicontinuous cubic phases with a maximal curvature deviator. However, other induced structures by pore-forming peptides such as inverted hexagonal phases have relatively high curvatures[71,72] that can be incorporated into the pore size estimations. Furthermore, we have assumed that the lipid bilayer is areally incompressible and that the system of membrane and peptides is in mechanical equilibrium. Future studies will focus on the effects of membrane dynamics, thermal fluctuations, and membrane stretching on the mechanism of pore formation by AMPs and CPPs. Additionally, the estimated pore sizes induced by AMPs (Table S2) depend on the lipid composition. For example, a previous experimental study reported pore formation by PG-1 with a 4.5 nm radius in DMPC bilayer patches,[22] while based on our calculations, PG-1 can induce transmembrane pores with a radius of ∼1.11 nm in a DOPS/DOPE (20/80) bilayer. Future studies will include the lipid composition for pore size estimation. Finally, induced deviatoric curvature is a simplified model to incorporate the induced NGC by pore former peptides while ignoring molecular mechanisms such as lipid tilts, peptide insertion, and the excluded volume effect for ions. Although it is effective for representing membrane remodeling due to membrane−peptide interactions, future efforts focusing on different molecular aspects of NGC generation will be important for designing the next generation of pore-forming systems.

## METHODS

The complete derivations with details are given in the Supporting Information.

## ASSOCIATED CONTENT

### Supporting Information

The Supporting Information is available free of charge at https://pubs.acs.org/doi/10.1021/jacs.3c08014.

Complete derivations with details; surface area of peptides, cubic lattice constant, estimated pore sizes, and the reported pore size induced by each peptide in the literature (Table S2); shows the nonmonotonic behavior of pore radius as a function of cubic lattice constant (Figure S1), and SAXS intensity profile for magainin (Figure S2) (PDF)

## AUTHOR INFORMATION


### Corresponding Author

**Gerard C. L. Wong** − *Department of Bioengineering, University of California, Los Angeles, Los Angeles, California 90025, United States; Department of Chemistry and Biochemistry, Department of Microbiology, Immunology, and Molecular Genetics, and California NanoSystems Institute, University of California, Los Angeles, California 90095, United States;* orcid.org/0000-0003-0893-6383; Email: gclwong@seas.ucla.edu

### Authors

**Haleh Alimohamadi** − *Department of Bioengineering, University of California, Los Angeles, Los Angeles, California 90025, United States; Department of Chemistry and Biochemistry, Department of Microbiology, Immunology, and Molecular Genetics, and California NanoSystems Institute, University of California, Los Angeles, California 90095, United States;* orcid.org/0000-0001-6576-2426

**Jaime de Anda** − *Department of Bioengineering, University of California, Los Angeles, Los Angeles, California 90025, United States; Department of Chemistry and Biochemistry, Department of Microbiology, Immunology, and Molecular Genetics, and California NanoSystems Institute, University of California, Los Angeles, California 90095, United States;* orcid.org/0000-0003-2129-0775

**Michelle W. Lee** − *Department of Bioengineering, University of California, Los Angeles, Los Angeles, California 90025, United States;* orcid.org/0000-0003-1613-9501

**Nathan W. Schmidt** − *Department of Bioengineering, University of California, Los Angeles, Los Angeles, California 90025, United States;* Present Address: Ginkgo Bioworks, Boston, Massachusetts 02210, United States

**Taraknath Mandal** − *Department of Physics, Indian Institute of Technology Kanpur, Kanpur 208016, India*

Complete contact information is available at:

https://pubs.acs.org/10.1021/jacs.3c08014

### Notes

The authors declare no competing financial interest.

## ■ ACKNOWLEDGMENTS

The authors thank Dennis Bong for the generous gift of magainin peptide. This work was supported by American Heart Association (AHA 966662) grant to G.C.L.W. H.A. was supported by the Vascular Biology Training Grant (T32 HL069766-21), and J.D.A. was supported by NSF Graduate Research Fellowship Program (DGE-1650604). T.M. gratefully acknowledges the support from the Government of India: Science and Engineering Research Board via Sanction No. SRG/2022/000548. The authors thank the Stanford Synchrotron Radiation Lightsource (SSRL) (Menlo Park, CA) for access to beamline 4-2. Use of the SSRL, SLAC National Accelerator Laboratory, is supported by the U.S. Department of Energy, Office of Science, Office of Basic Energy Sciences under contract no. DE-AC02-76SF00515. The SSRL Structural Molecular Biology Program is supported by the U.S. Department of Energy, Office of Biological and Environmental Research, and by the National Institutes of Health, National Institute of General Medical Sciences (including P30GM133894). T.M. is grateful for the computational resources provided by PARAM Sanganak under the National Supercomputing Mission, Government of India, at the Indian Institute of Technology, Kanpur.

## ■ REFERENCES

(1) Zasloff, M. Antimicrobial Peptides of Multicellular Organisms. *Nature* **2002**, *415* (6870), 389−395.
(2) Brogden, K. A. Antimicrobial Peptides: Pore Formers or Metabolic Inhibitors in Bacteria? *Nat. Rev. Microbiol.* **2005**, *3* (3), 238−250.
(3) Yu, Y.; Vroman, J. A.; Bae, S. C.; Granick, S. Vesicle Budding Induced by a Pore-Forming Peptide. *J. Am. Chem. Soc.* **2010**, *132* (1), 195−201.
(4) Shai, Y. Mechanism of the Binding, Insertion and Destabilization of Phospholipid Bilayer Membranes by α-Helical Antimicrobial and Cell Non-Selective Membrane-Lytic Peptides. *Biochim. Biophys. Acta, Biomembr.* **1999**, *1462* (1), 55−70.
(5) Youle, R. J.; Strasser, A. The BCL-2 Protein Family: Opposing Activities That Mediate Cell Death. *Nat. Rev. Mol. Cell Biol.* **2008**, *9* (1), 47−59.
(6) Silvestre-Roig, C.; Braster, Q.; Wichapong, K.; Lee, E. Y.; Teulon, J. M.; Berrebeh, N.; Winter, J.; Adrover, J. M.; Santos, G. S.; Froese, A.; Lemnitzer, P.; Ortega-Gómez, A.; Chevre, R.; Marschner, J.; Schumski, A.; Winter, C.; Perez-Olivares, L.; Pan, C.; Paulin, N.; Schoufour, T.; Hartwig, H.; González-Ramos, S.; Kamp, F.; Megens, R. T. A.; Mowen, K. A.; Gunzer, M.; Maegdefessel, L.; Hackeng, T.; Lutgens, E.; Daemen, M.; von Blume, J.; Anders, H.-J.; Nikolaev, V. O.; Pellequer, J.-L.; Weber, C.; Hidalgo, A.; Nicolaes, G. A. F.; Wong, G. C. L.; Soehnlein, O. Externalized Histone H4 Orchestrates Chronic Inflammation by Inducing Lytic Cell Death. *Nature* **2019**, *569* (7755), 236−240.
(7) Beckett, A. J.; Prior, I. A. Electron Microscopy Methods for Studying Plasma Membranes. *Methods Mol. Biol.* **2015**, *1232*, 137−151.
(8) Epand, R. M.; Vogel, H. J. Diversity of Antimicrobial Peptides and Their Mechanisms of Action. *Biochim. Biophys. Acta, Biomembr.* **1999**, *1462* (1), 11−28.
(9) Robson, A.-L.; Dastoor, P. C.; Flynn, J.; Palmer, W.; Martin, A.; Smith, D. W.; Woldu, A.; Hua, S. Advantages and Limitations of Current Imaging Techniques for Characterizing Liposome Morphology. *Front. Pharmacol.* **2018**, *9* (8), No. 80.
(10) Mishra, A.; Lai, G. H.; Schmidt, N. W.; Sun, V. Z.; Rodriguez, A. R.; Tong, R.; Tang, L.; Cheng, J.; Deming, T. J.; Kamei, D. T.; Wong, G. C. L. Translocation of HIV TAT Peptide and Analogues Induced by Multiplexed Membrane and Cytoskeletal Interactions. *Proc. Natl. Acad. Sci. U.S.A.* **2011**, *108* (41), 16883−16888.
(11) Lee, M. W.; Lee, E. Y.; Lai, G. H.; Kennedy, N. W.; Posey, A. E.; Xian, W.; Ferguson, A. L.; Hill, R. B.; Wong, G. C. L. Molecular Motor Dnm1 Synergistically Induces Membrane Curvature To Facilitate Mitochondrial Fission. *ACS Cent. Sci.* **2017**, *3* (11), 1156−1167.
(12) Schmidt, N. W.; Mishra, A.; Wang, J.; DeGrado, W. F.; Wong, G. C. L. Influenza Virus A M2 Protein Generates Negative Gaussian Membrane Curvature Necessary for Budding and Scission. *J. Am. Chem. Soc.* **2013**, *135* (37), 13710−13719.
(13) Schmidt, N. W.; Mishra, A.; Lai, G. H.; Davis, M.; Sanders, L. K.; Tran, D.; Garcia, A.; Tai, K. P.; McCray, P. B.; Ouellette, A. J.; Selsted, M. E.; Wong, G. C. L. Criterion for Amino Acid Composition of Defensins and Antimicrobial Peptides Based on Geometry of Membrane Destabilization. *J. Am. Chem. Soc.* **2011**, *133* (17), 6720−6727.
(14) Lee, M. W.; Luo, E. W.-C.; Silvestre-Roig, C.; Srinivasan, Y.; Akabori, K.; Lemnitzer, P.; Schmidt, N. W.; Lai, G. H.; Santangelo, C. D.; Soehnlein, O.; Wong, G. C. L. Apolipoprotein Mimetic Peptide Inhibits Neutrophil-Driven Inflammatory Damage via Membrane Remodeling and Suppression of Cell Lysis. *ACS Nano* **2021**, *15* (10), 15930−15939.
(15) Schmidt, N. W.; Tai, K. P.; Kamdar, K.; Mishra, A.; Lai, G. H.; Zhao, K.; Ouellette, A. J.; Wong, G. C. L. Arginine in α-Defensins: Differential Effects on Bactericidal Activity Correspond to Geometry of Membrane Curvature Generation and Peptide-lipid Phase Behavior *. *J. Biol. Chem.* **2012**, *287* (26), 21866−21872.
(16) Schmidt, N. W.; Wong, G. C. Antimicrobial Peptides and Induced Membrane Curvature: Geometry, Coordination Chemistry, and Molecular Engineering. *Curr. Opin. Solid State Mater. Sci.* **2013**, *17* (4), 151−163.
(17) Lohner, K.; Prenner, E. J. Differential Scanning Calorimetry and X-Ray Diffraction Studies of the Specificity of the Interaction of Antimicrobial Peptides with Membrane-Mimetic Systems. *Biochim. Biophys. Acta, Biomembr.* **1999**, *1462* (1), 141−156.
(18) Hickel, A.; Danner-Pongratz, S.; Amenitsch, H.; Degovics, G.; Rappolt, M.; Lohner, K.; Pabst, G. Influence of Antimicrobial Peptides on the Formation of Nonlamellar Lipid Mesophases. *Biochim. Biophys. Acta, Biomembr.* **2008**, *1778* (10), 2325−2333.
(19) Leal, C.; Bouxsein, N. F.; Ewert, K. K.; Safinya, C. R. Highly Efficient Gene Silencing Activity of siRNA Embedded in a Nanostructured Gyroid Cubic Lipid Matrix. *J. Am. Chem. Soc.* **2010**, *132* (47), 16841−16847.
(20) Kim, H.; Leal, C. Cuboplexes: Topologically Active siRNA Delivery. *ACS Nano* **2015**, *9* (10), 10214−10226.
(21) Alimohamadi, H.; Rangamani, P. Modeling Membrane Curvature Generation Due to Membrane−Protein Interactions. *Biomolecules* **2018**, *8* (4), No. 120.
(22) Lam, K. L. H.; Wang, H.; Siaw, T. A.; Chapman, M. R.; Waring, A. J.; Kindt, J. T.; Lee, K. Y. C. Mechanism of Structural Transformations Induced by Antimicrobial Peptides in Lipid Membranes. *Biochim. Biophys. Acta, Biomembr.* **2012**, *1818* (2), 194−204.
(23) Cunill-Semanat, E.; Salgado, J. Spontaneous and Stress-Induced Pore Formation in Membranes: Theory, Experiments and Simulations. *J. Membr. Biol.* **2019**, *252* (4), 241−260.
(24) Ting, C. L.; Awasthi, N.; Müller, M.; Hub, J. S. Metastable Prepores in Tension-Free Lipid Bilayers. *Phys. Rev. Lett.* **2018**, *120* (12), No. 128103.
(25) Siegel, D. P. Bicontinuous Inverted Cubic Phase Stabilization as an Index of Antimicrobial and Membrane Fusion Peptide Activity. *Biochim. Biophys. Acta, Biomembr.* **2022**, *1864* (1), No. 183815.
(26) Golani, G.; Schwarz, U. S. High Curvature Promotes Fusion of Lipid Membranes: Predictions from Continuum Elastic Theory. *Biophys. J.* **2023**, *122* (10), 1868−1882.

(27) Bennett, W. F. D.; Hong, C. K.; Wang, Y.; Tieleman, D. P. Antimicrobial Peptide Simulations and the Influence of Force Field on the Free Energy for Pore Formation in Lipid Bilayers. *J. Chem. Theory Comput.* **2016**, *12* (9), 4524−4533.
(28) Sengupta, D.; Leontiadou, H.; Mark, A. E.; Marrink, S.-J. Toroidal Pores Formed by Antimicrobial Peptides Show Significant Disorder. *Biochim. Biophys. Acta, Biomembr.* **2008**, *1778* (10), 2308−2317.
(29) Leontiadou, H.; Mark, A. E.; Marrink, S. J. Antimicrobial Peptides in Action. *J. Am. Chem. Soc.* **2006**, *128* (37), 12156−12161.
(30) Alimohamadi, H.; Rangamani, P. Effective Cell Membrane Tension Protects Red Blood Cells against Malaria Invasion *bioRxiv* 2023.
(31) Akimov, S. A.; Volynsky, P. E.; Galimzyanov, T. R.; Kuzmin, P. I.; Pavlov, K. V.; Batishchev, O. V. Pore Formation in Lipid Membrane I: Continuous Reversible Trajectory from Intact Bilayer through Hydrophobic Defect to Transversal Pore. *Sci. Rep.* **2017**, *7* (1), No. 12152.
(32) Akimov, S. A.; Volynsky, P. E.; Galimzyanov, T. R.; Kuzmin, P. I.; Pavlov, K. V.; Batishchev, O. V. Pore Formation in Lipid Membrane II: Energy Landscape under External Stress. *Sci. Rep.* **2017**, *7* (1), No. 12509.
(33) Fošnarič, M.; Kralj-Iglič, V.; Bohinc, K.; Iglič, A.; May, S. Stabilization of Pores in Lipid Bilayers by Anisotropic Inclusions. *J. Phys. Chem. B* **2003**, *107* (45), 12519−12526.
(34) Betterton, M. D.; Brenner, M. P. Electrostatic Edge Instability of Lipid Membranes. *Phys. Rev. Lett.* **1999**, *82* (7), 1598−1601.
(35) Mihajlovic, M.; Lazaridis, T. Antimicrobial Peptides Bind More Strongly to Membrane Pores. *Biochim. Biophys. Acta, Biomembr.* **2010**, *1798* (8), 1494−1502.
(36) Rawicz, W.; Olbrich, K. C.; McIntosh, T.; Needham, D.; Evans, E. Effect of Chain Length and Unsaturation on Elasticity of Lipid Bilayers. *Biophys. J.* **2000**, *79* (1), 328−339.
(37) Helfrich, W. Elastic Properties of Lipid Bilayers: Theory and Possible Experiments. *Z. Naturforsch. C* **1973**, *28* (11), 693−703.
(38) Alimohamadi, H.; Smith, A. S.; Nowak, R. B.; Fowler, V. M.; Rangamani, P. Non-Uniform Distribution of Myosin-Mediated Forces Governs Red Blood Cell Membrane Curvature through Tension Modulation. *PLoS Comput. Biol.* **2020**, *16* (5), No. e1007890.
(39) Iglič, A.; Slivnik, T.; Kralj-Iglič, V. Elastic Properties of Biological Membranes Influenced by Attached Proteins. *J. Biomech.* **2007**, *40* (11), 2492−2500.
(40) Kralj-Iglič, V.; Heinrich, V.; Svetina, S.; Žekš, B. Free Energy of Closed Membrane with Anisotropic Inclusions. *Eur. Phys. J. B* **1999**, *10*, 5−8.
(41) Alimohamadi, H.; Bell, M. K.; Halpain, S.; Rangamani, P. Mechanical Principles Governing the Shapes of Dendritic Spines. *Front. Physiol.* **2021**, *12*, No. 657074.
(42) Alberts, B.; Johnson, A.; Lewis, J.; Raff, M.; Roberts, K.; Walter, P. The Cytoskeleton and Cell Behavior. In *Molecular Biology of the Cell*, 4th ed.; Garland Science, 2002.
(43) Alimohamadi, H.; Ovryn, B.; Rangamani, P. Modeling Membrane Nanotube Morphology: The Role of Heterogeneity in Composition and Material Properties. *Sci. Rep.* **2020**, *10* (1), No. 2527.
(44) Alimohamadi, H. *Application of Continuum Mechanics for a Variety of Curvature Generation Phenomena in Cell Biophysics*; University of California: San Diego, 2021.
(45) Alimohamadi, H.; Vasan, R.; Hassinger, J.; Stachowiak, J.; Rangamani, P. The Role of Traction in Membrane Curvature Generation. *Biophys. J.* **2018**, *114* (3), No. 600a.
(46) Lipowsky, R. Budding of Membranes Induced by Intramembrane Domains. *J. Phys. II* **1992**, *2* (10), 1825−1840.
(47) Shigematsu, T.; Koshiyama, K.; Wada, S. Line Tension of the Pore Edge in Phospholipid/Cholesterol Bilayer from Stretch Molecular Dynamics Simulation. *J. Biomech. Sci. Eng.* **2015**, *11*, 15−00422.
(48) Baumgart, T.; Hess, S. T.; Webb, W. W. Imaging Coexisting Fluid Domains in Biomembrane Models Coupling Curvature and Line Tension. *Nature* **2003**, *425* (6960), 821−824.
(49) May, S. A Molecular Model for the Line Tension of Lipid Membranes. *Eur. Phys. J. E* **2000**, *3* (1), 37−44.
(50) Henderson, J. M.; Waring, A. J.; Separovic, F.; Lee, K. Y. C. Antimicrobial Peptides Share a Common Interaction Driven by Membrane Line Tension Reduction. *Biophys. J.* **2016**, *111* (10), 2176−2189.
(51) Israelachvili, J. N. *Intermolecular and Surface Forces*; Academic Press, 2011.
(52) Bossa, G. V.; May, S. Debye-Hückel Free Energy of an Electric Double Layer with Discrete Charges Located at a Dielectric Interface. *Membranes* **2021**, *11* (2), No. 129.
(53) Harper, P. E.; Gruner, S. M. Electron Density Modeling and Reconstruction of Infinite Periodic Minimal Surfaces (IPMS) Based Phases in Lipid-Water Systems. I. Modeling IPMS-Based Phases. *Eur. Phys. J. E* **2000**, *2* (3), 217−228.
(54) Schwarz, U. S.; Gompper, G. Systematic Approach to Bicontinuous Cubic Phases in Ternary Amphiphilic Systems. *Phys. Rev. E* **1999**, *59* (5), 5528−5541.
(55) Basañez, G.; Soane, L.; Hardwick, J. M. A New View of the Lethal Apoptotic Pore. *PLoS Biol.* **2012**, *10* (9), No. e1001399.
(56) Kondrashov, O. V.; Kuzmin, P. I.; Akimov, S. A. Pore Formation by Amphipathic Peptides in Closed Membranes. *Biochem. (Moscow), Suppl. Ser.* **2022**, *16* (4), 328−337.
(57) Khunpetch, P.; Majee, A.; Podgornik, R. Curvature Effects in Charge-Regulated Lipid Bilayers. *Soft Matter* **2022**, *18* (13), 2597−2610.
(58) Shojaei, H. R.; Božič, A. L.; Muthukumar, M.; Podgornik, R. Effects of Long-Range Interactions on Curvature Energies of Viral Shells. *Phys. Rev. E* **2016**, *93* (5), No. 052415.
(59) Karatekin, E.; Sandre, O.; Guitouni, H.; Borghi, N.; Puech, P.-H.; Brochard-Wyart, F. Cascades of Transient Pores in Giant Vesicles: Line Tension and Transport. *Biophys. J.* **2003**, *84* (3), 1734−1749.
(60) Moroz, J. D.; Nelson, P. Dynamically Stabilized Pores in Bilayer Membranes. *Biophys. J.* **1997**, *72* (5), 2211−2216.
(61) Raguse, T. L.; Porter, E. A.; Weisblum, B.; Gellman, S. H. Structure−Activity Studies of 14-Helical Antimicrobial $\beta$-Peptides: Probing the Relationship between Conformational Stability and Antimicrobial Potency. *J. Am. Chem. Soc.* **2002**, *124* (43), 12774−12785.
(62) Liu, D.; DeGrado, W. F. De Novo Design, Synthesis, and Characterization of Antimicrobial $\beta$-Peptides. *J. Am. Chem. Soc.* **2001**, *123* (31), 7553−7559.
(63) Schmitt, M. A.; Weisblum, B.; Gellman, S. H. Unexpected Relationships between Structure and Function in $\alpha,\beta$-Peptides: Antimicrobial Foldamers with Heterogeneous Backbones. *J. Am. Chem. Soc.* **2004**, *126* (22), 6848−6849.
(64) Herce, H. D.; Garcia, A. E.; Litt, J.; Kane, R. S.; Martin, P.; Enrique, N.; Rebolledo, A.; Milesi, V. Arginine-Rich Peptides Destabilize the Plasma Membrane, Consistent with a Pore Formation Translocation Mechanism of Cell-Penetrating Peptides. *Biophys. J.* **2009**, *97* (7), 1917−1925.
(65) Takeshima, K.; Chikushi, A.; Lee, K.-K.; Yonehara, S.; Matsuzaki, K. Translocation of Analogues of the Antimicrobial Peptides Magainin and Buforin across Human Cell Membranes *. *J. Biol. Chem.* **2003**, *278* (2), 1310−1315.
(66) Yang, L.; Harroun, T. A.; Weiss, T. M.; Ding, L.; Huang, H. W. Barrel-Stave Model or Toroidal Model? A Case Study on Melittin Pores. *Biophys. J.* **2001**, *81* (3), 1475−1485.
(67) Cirac, A. D.; Moiset, G.; Mika, J. T.; Koçer, A.; Salvador, P.; Poolman, B.; Marrink, S. J.; Sengupta, D. The Molecular Basis for Antimicrobial Activity of Pore-Forming Cyclic Peptides. *Biophys. J.* **2011**, *100* (10), 2422−2431.
(68) Ciobanasu, C.; Siebrasse, J. P.; Kubitscheck, U. Cell-Penetrating HIV1 TAT Peptides Can Generate Pores in Model Membranes. *Biophys. J.* **2010**, *99* (1), 153−162.


https://doi.org/10.1021/jacs.3c08014
J. Am. Chem. Soc. 2023, 145, 26095−26105

(69) Yao, H.; Lee, M. W.; Waring, A. J.; Wong, G. C.; Hong, M. Viral Fusion Protein Transmembrane Domain Adopts β-Strand Structure to Facilitate Membrane Topological Changes for Virus−Cell Fusion. *Proc. Natl. Acad. Sci. U.S.A.* **2015**, *112* (35), 10926−10931.
(70) Lee, M.; Morgan, C. A.; Hong, M. Fully Hydrophobic HIV Gp41 Adopts a Hemifusion-like Conformation in Phospholipid Bilayers. *J. Biol. Chem.* **2019**, *294* (40), 14732−14744.
(71) Perutková, Š.; Daniel, M.; Rappolt, M.; Pabst, G.; Dolinar, G.; Kralj-Iglič, V.; Iglič, A. Elastic Deformations in Hexagonal Phases Studied by Small-Angle X-Ray Diffraction and Simulations. *Phys. Chem. Chem. Phys.* **2011**, *13* (8), 3100−3107.
(72) Rappolt, M.; Hodzic, A.; Sartori, B.; Ollivon, M.; Laggner, P. Conformational and Hydrational Properties during the Lβ- to Lα- and Lα- to HII-Phase Transition in Phosphatidylethanolamine. *Chem. Phys. Lipids* **2008**, *154* (1), 46−55.



https://doi.org/10.1021/jacs.3c08014
*J. Am. Chem. Soc.* 2023, 145, 26095−26105